European Journal of Nuclear Medicine and Molecular Imaging
https://doi.org/10.1007/s00259-023-06115-5

ORIGINAL ARTICLE

An ultra-small bispecific protein augments tumor penetration and treatment for pancreatic cancer

Qian Wang[1] · Jingyun Wang[2] · Hao Yan[3,6] · Zheng Li[4] · Kun Wang[5] · Feiyu Kang[6] · Jie Tian[5] · Xinming Zhao[1] · Seok-Hyun Yun[3]

Received: 21 October 2022 / Accepted: 11 January 2023

Abstract

Purpose The once highly anticipated antibody-based pathway-targeted therapies have not achieved promising outcomes for deadly pancreatic ductal adenocarcinoma (PDAC), mainly due to drugs' low intrinsic anticancer activity and poor penetration across the dense physiological barrier. This study aims to develop an ultra-small-sized, EGFR/VEGF bispecific therapeutic protein to largely penetrate deep tumor tissue and effectively inhibit PDAC tumor growth in vivo.

Methods The bispecific protein, Bi-fp50, was constructed by a typical synthetic biology method and labeled with fluorescent dyes for in vitro and in vivo imaging. Physicochemical properties, protein dual-binding affinity, and specificity of the Bi-fp50 were evaluated in several PDAC cell lines. In vitro quantitatively and qualitatively anticancer activity of Bi-fp50 was assessed by live/dead staining, MTT assay, and flow cytometry. In vivo pharmacokinetic and biodistribution were evaluated using blood biopsy samples and near-infrared fluorescence imaging. In vivo real-time tracking of Bi-fp50 in the local tumor was conducted by fibered confocal fluorescence microscopy. The subcutaneous PDAC tumor model was used to assess the in vivo antitumor effect of Bi-fp50.

Results Bi-fp50 with an ultra-small size of 50 kDa (5 ~ 6 nm) showed an excellent binding ability to VEGF and EGFR simultaneously and had enhanced, accumulated binding capability for Bxpc3 PDAC cells compared with anti-VEGF scFv and anti-EGFR scFv alone. Additionally, bi-fp50 significantly inhibited the proliferation and growth of Bxpc3 and Aspc1 PDAC cells even under a relatively low concentration (0.3 μM). It showed synergistically enhanced therapeutic effects relative to two individual scFv and Bi-fp50x control in vitro. The half-life of blood clearance of Bi-fp50 was 4.33 ± 0.23 h. After intravenous injection, Bi-fp50 gradually penetrated the deep tumor, widely distributed throughout the whole tissue, and primarily enriched in the tumor with nearly twice the accumulation than scFv2 in the orthotopic PDAC tumor model. Furthermore, the Bi-fp50 protein could induce broad apoptosis in the whole tumor and significantly inhibited tumor growth 3 weeks after injection in vivo without other noticeable side effects.

Conclusion The proof-of-concept study demonstrated that the ultra-small-sized, bispecific protein Bi-fp50 could be a potential tumor suppressor and an efficient, safe theranostic tool for treating PDAC tumors.

Keywords Bispecific antibody · PDAC therapy · Molecular imaging · Synthetic biology

Introduction

Pancreatic cancer therapy currently remains a formidable challenge. The overall 5-year survival for pancreatic cancer, mainly comprising pancreatic ductal adenocarcinoma (PDAC), has changed little over the past decade [1, 2]. Conventional treatments such as surgery, FOLFIRINOX-based chemotherapy, and radiotherapy can prolong the survival of patients in specific stages of PDAC [3–7]. However, their specificity is limited, which would dramatically affect the therapeutic effect and usually incur severe side effects. Highly specific monoclonal antibodies (mAbs)-based pathway-targeted therapies

Qian Wang and Jingyun Wang contributed equally to this work.

This article is part of the Topical Collection on Oncology - General.

✉ Hao Yan
hyan23@sz.tsinghua.edu.cn

✉ Jie Tian
jie.tian@ia.ac.cn

✉ Xinming Zhao
xinmingzh2017@yeah.net

Extended author information available on the last page of the article

Published online: 24 January 2023

once had high hopes and had been widely evaluated alone or combined with chemotherapy in PDAC treatment [8, 9], but unfortunately, failed to improve patient survival [10, 11]. It was speculated that the low intrinsic efficacy of mono-targeted drugs owing to the exceptionally high molecular heterogeneity of PDAC cells is one of the main reasons [4, 12, 13]. Recently, multispecific therapeutic agents that engage two or more targeting entities are believed to be more suitable for highly heterogeneous cancer cells [14, 15] and have shown enhanced or synergistic therapeutic effects for various cancer in the clinic [16, 17]. Therefore, developing highly multispecific therapeutic agents may be an effective and promising way to improve the therapeutic efficacy of PDAC.

Epidermal growth factor receptor (EGFR) is overexpressed in more than 90% of patients' PDAC, and signaling via it could regulate the growth, proliferation, and apoptosis of PDACs [13, 18]. Vascular endothelial growth factor (VEGF) is another overexpressed target in 64% of PDAC and has been recognized as a critical mediator of angiogenesis [19]. Interestingly, substantial preclinical studies and multiple clinical trials in several cancer diseases all suggest that the EGFR and VEGF pathways are interrelated, and dual EGFR-VEGF pathway inhibition could delay acquired resistance of anti-EGFR or anti-VEGF used alone [20–22]. Moreover, treating PDAC tumor vasculature by targeting VEGF can develop a "vessel-normalization window" and reduce the tumoral interstitial fluid pressure (IFP) [23, 24], thus facilitating the penetration of other targeting molecules. Therefore, it's reasonable to hypothesize that dual inhibition of EGFR-VEGF pathways of PDAC cells simultaneously may delay the individual resistance and achieve an enhanced or synergistic therapeutic effect, a strategy that has not been achieved for PDACs, according to our knowledge.

Moreover, the unique physiological barriers of PDAC tumors, especially the extremely dense desmoplastic stroma and the increased interstitial fluid pressure, are decisive factors affecting the drug delivery efficacy in vivo [4, 12, 13, 25]. The small size, especially under dozens of kDa, was critical for therapeutic agents to overcome the dense pathophysiological barriers to enrich PDAC tumors [13, 26–28]. The traditional direct conjugation of two or more mAbs would result in an overall large size, which is not conducive for therapeutic agents to penetrate deeply and widely in PDAC tumors [26–28]. Multispecific fusion proteins can retain all the specificity while having several times the smaller molecular size and thus have been successfully used for in vivo molecular imaging recently [28–30]. Herein, we developed an ultra-small-sized, bispecific fusion protein, Bi-fp50, that could simultaneously target EGFR-VEGF pathways for PDACs and efficiently extravasate through the dense barriers to accumulate in deep tumor tissue by typical synthetic biology method (Scheme 1). Physicochemical properties, protein dual-binding affinity, and specificity of the Bi-fp50 were evaluated in several PDAC cell lines. In vivo pharmacokinetic, biodistribution, and real-time local tracking of Bi-fp50 were evaluated using near-infrared fluorescence imaging. In vitro and in vivo quantitatively and qualitatively, the anticancer activity of Bi-fp50 was further assessed in several human PDAC cell lines and PDAC tumors. This study aims to construct an ultra-small-sized multispecific protein that can provide a new strategy for more effective targeted pathway therapy for PDAC in vivo.

Materials and methods

Preparation of bispecific fusion protein Bi-fp50

As with the previous procedure [28], we first screened and selected anti-VEGF and anti-EGFR antibodies with high specificity to PDAC cells from a natural antibody library. Then, the corresponding gene sequence, which can express single-chain variable fragments (scFvs) of anti-EGFR and anti-VEGF, was constructed and transfected into engineered bacteria *E. coli* by genetic engineering method. After lysis and purification, the Bi-fp50 was obtained. In addition, the control protein scFv2 was obtained by directly connecting two scFv (anti-EGFR scFv and anti-VEGF scFv) together through a linker $(GGGGS)_3$ as the sequence of V_L1-linker-V_H1-linker-V_L2-linker-V_H2. And another control protein, Bi-fp50x, which has all the structural features of Bi-fp50 but does not have the binding function of Bi-fp50, was produced by the same synthetic biology method as Bi-fp50.

Characteristics of Bi-fp50

Sodium dodecyl sulfate–polyacrylamide gel electrophoresis (SDS-PAGE) was used to study the molecule weight of Bi-fp50, anti-EGFR scFv, and anti-VEGF scFv. The Fourier transform infrared spectra (FTIR) was used to characterize the structure of Bi-fp50. Meanwhile, the enzyme-linked immunosorbent assay (ELISA) assay was carried out to compare the binding affinities of Bi-fp50 with anti-EGFR scFv, anti-VEGF scFv, scFv2, and Bi-fp50x. First, Human recombinant EGFR or/and VEGF were coated on 96-well plates at 4 °C for 24 h. Then, the plates were incubated with either protein at 37 °C for 2 h, followed by incubation with the anti-Human IgG (Fab specific) – Peroxidase antibody (Sigma). After reaction with 3,3′,5,5′-tetramethylbenzidine (TMB), the binding affinity of these proteins were identified by testing the absorbance at 450 nm. Rabbit mono/polyclonal antibodies against EGFR, VEGF, GAPDH, STAT3, p-STAT3, AKT, p-AKT, and β-actin were used for the western blotting analysis of Bi-fp50 following typical standard protocol.

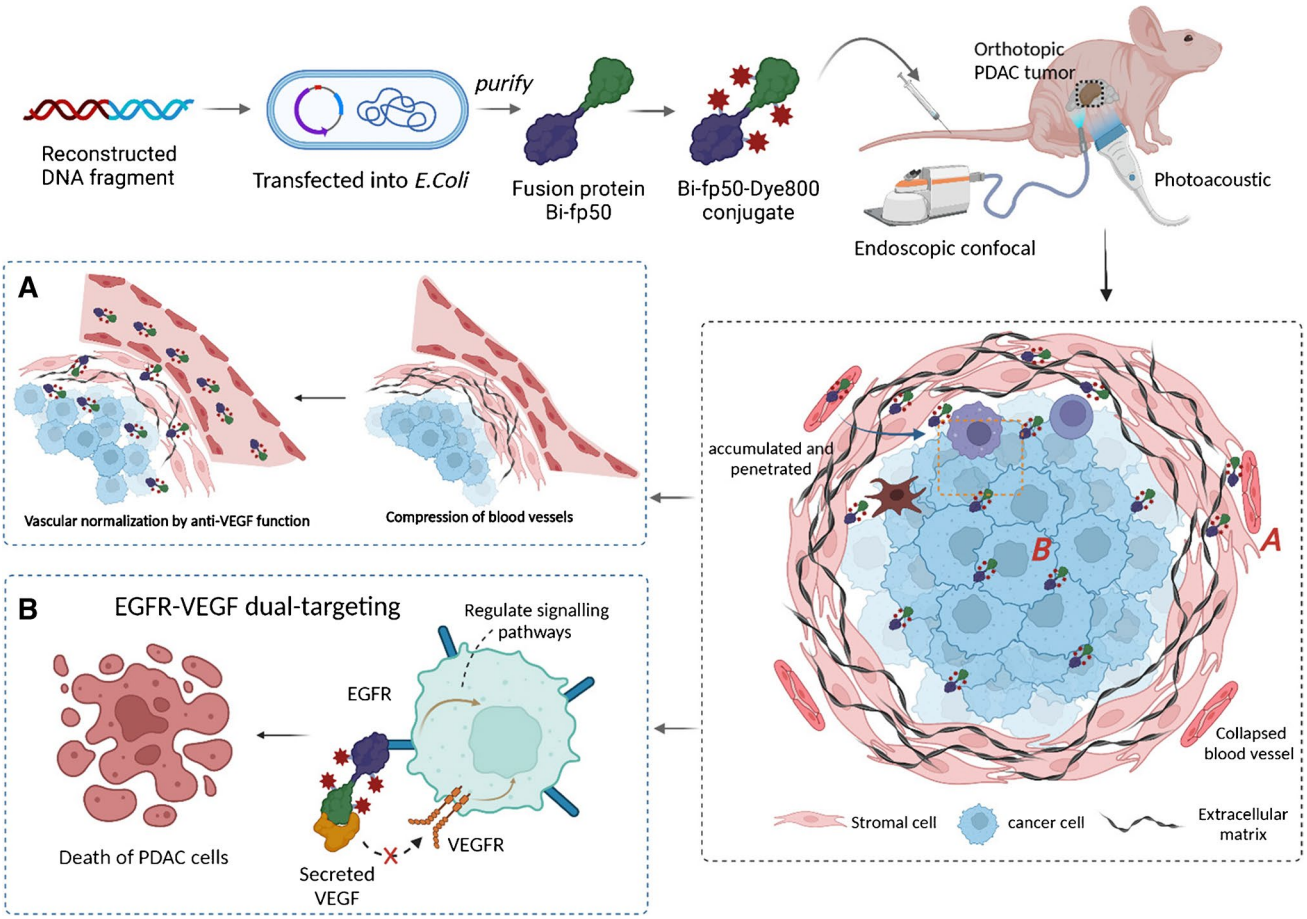

Scheme 1 Schematic illustration of the construction of the bispecific protein Bi-fp50 and its expected tumor penetration and targeted therapy against pancreatic cancer. The anti-VEGF function of Bi-fp50 could normalize the vessel structure of the tumor and reduce interstitial fluid pressure, along with its ultra-small size together enhance intra-tumoral penetration and accumulation. In addition, dual targeting of EGFR and VEGF produced apoptosis of PDACs

Cell culture and in vitro *targeting experiments*

The human pancreatic ductal adenocarcinoma cell lines Bxpc3, Aspc1, Panc1, SW1990, Capan2, T3M4, and HPDE6-C7 human pancreatic duct epithelial cells were purchased from ATCC. All cell lines were cultured in Dulbecco's modified Eagle medium (DMEM) (HyClone) with 10% fetal bovine serum FBS (HyClone) and 1% penicillin–streptomycin (PS) (Promega) at 37 °C in a 5% CO_2 atmosphere.

EGFR and VEGF expression for different PDAC cells were determined by Western blotting assay. Six kinds of pancreatic cancer cells were harvested during the exponential phase and lysed in 1 × PBS, 1% Nonidet P-40 (Thermo Scientific), 2 μg ml^{-1} Aprotinin, 2 μg ml^{-1} Leupeptin, and 50 μg ml^{-1} phenylmethylsulfonyl fluoride (PMSF). After centrifuging at 12,000 g at 4 °C for 10 min, the total proteins were extracted from the supernatants and then quantified using the Pierce BCA assay kit. Next, proteins were separated through SDS-PAGE (10% resolving gel) and electroblotted onto a polyvinylidene fluoride (PVDF) membrane using the semi-dry blotting system (Bio-rad). Next, the membrane was blocked with 1 × PBST buffer for 30 min, incubated with anti-EGFR and anti-VEGF (Abcam) at a concentration ratio of 1:1000, respectively. After that, the anti-rabbit secondary antibodies at 1:2000 were conjugated with horseradish peroxidase. Chemiluminescence signals were detected using ImageQuant LAS 4000 (GE Healthcare Life Sciences).

The targeting properties of Bi-fp50 were further studied. The Bi-fp50, scFvs, and two anti-VEGF scFv and Bi-fp50x were labeled with Alexa Fluor 488 (AF488) separately to visualize the protein. After incubating different protein probes (0.05 μM) for 2 h, Bxpc3 cells were fixed and stained by DAPI (4′,6-diamidino-2-phenylindole). Confocal microscopy was used to image the cellular targeting of protein probes. Image J software was further used for quantitative analysis.

In vitro *anticancer ability assessment of Bi-fp50*

Three different cell lines (HPDE6-C7, Bxpc3, and Axpc1) were used to study the anticancer effect of Bi-fp50. Cells were first seeded on 96-well plates and cultured for another 24 h. Then, anti-EGFR scFv, anti-VEGF scFv, and Bi-fp50 with different concentrations were added to the culture plates and co-incubated at 37 °C for another 24 h, respectively. Finally, MTT (3-(4,5-dimethylthiazol-2-yl)-2,5-diphenyltetrazolium bromide) solution was added to each well incubated for 4 h at 37 °C to study the cell viability. For live/dead staining assay, 24 h after being co-incubated with a different protein, the Bxpc3 cells were stained by Calcein–AM and propidium iodide (PI). The experiment was performed in triple technical replicates and standardized. For apoptosis analysis, the Bi-fp50 and other control proteins were first co-incubated with Bxpc3 cells for 48 h. Then the cells were stained by an annexin V-FITC apoptosis detection kit. Briefly, the cells were suspended in 5 μL of annexin V-FITC and 195 μL of annexin V-FITC binding buffer and incubated for 10 min. After centrifuging for 5 min, the cells were re-suspended in 190 μL of binding buffer and 10 μL of propidium iodide (PI) working solution. The flow cytometric method was finally carried out to analyze the staining results.

Animals and PDAC tumor model

Animal experiments were performed in compliance with the Animal Ethics Committee of the Chinese Academy of Medical Sciences Tumor Hospital (#NCC2019A010). The whole study maintained strict adherence to protocols for animal care and use. Bxpc3-Luc (5×10^5 cells/mouse) cells were injected subcutaneously for the female BALB/C nude mice six weeks old. When subcutaneous tumors reached 5 mm, they were harvested and then chopped into 1 mm^3 piece. The small tumor masses were *implanted* in situ on the pancreas to form the orthotopic PDAC tumor model (for imaging) or injected into the subcutaneous to form a more subcutaneous PDAC tumor model (for therapy).

Blood clearance, biodistribution, and intra-tumoral penetration of Bi-fp50 in vivo

Bi-fp50 (or scFv2) was labeled with IRDye 800CW dye (Dye800) for in vivo imaging and analysis. In the blood clearance measurement, 10 μl of blood was harvested from the tail vein of Bxpc3-Luc tumor-bearing mice ($n = 3$) post-injection of Bi-fp50-Dye800 at different time points (10 min, 2, 4, 12, 24, and 48 h). The blood sample was immediately dissolved in 1 ml lysis buffer. And the concentration of the Bi-fp50-Dye800 in the blood was measured by the fluorescence spectrum with the Ex/Em at about 800 nm/820 nm. Then, a series of probe-blood dilutions were performed to obtain the standard calibration curve. Finally, a blank blood sample without Bi-fp50-Dye800 was measured to determine the blood autofluorescence level.

Bxpc3-Luc tumor-bearing mice ($n = 3$) were intravenously injected with Bi-fp50-Dye800 or scFv2-Dye800 separately (2 mg kg^{-1}), and fluorescent signals were detected at various time points by an IVIS imaging system (PerkinElmer). The fluorescence intensity under the same excitation at the ear of the mouse was used as the background to calculate the fluorescence signal of the probe-to-background ratio (SBR). The Bxpc3-Luc tumor-bearing mice ($n = 3$) were sacrificed at 4, 8, 12, and 24 h of post-injection for quantitative biodistribution analysis of protein in tissues. The major organs and tumors were weighed and homogenized in the lysis buffer and diluted 100 times. By measuring the fluorescence intensity of the probe in the tissue solution and comparing it with the standard calibration curve, the amount of the probe in tissues can be known. The samples were measured four times to ensure reproducibility and accuracy. Intra-tumoral penetration of Bi-fp50 and scFv2 was studied by a multispectral photoacoustic tomography system (iTheraMedical) with the 3D model of the photoacoustic imaging (PAI) device.

Real-time monitoring of the dynamics of Bi-fp50 in local PDAC tumor

The further intratumor penetration and dynamic distribution of Bi-fp50 in local tumor tissue were monitored by a fibered confocal fluorescence microscopy (FCFM) imaging system (Cellvizio). The orthotopic Bxpc3 tumor-bearing mice ($n = 3$) were intravenously injected with Bi-fp50-AF647 or scFv2-AF647 separately. FITC dyes were used to stain out the outline of the tissue. A flexible fiber mini probe connected to a 488/660 nm laser scanning unit was planted through a small incision in the abdomen to image the PDAC tumor and surrounding normal tissues. After imaging, the tumors were harvested and fixed in 4% paraformaldehyde and then embedded and cut into ~ 10 μm cryosections for further histological analysis.

Antitumor effect of Bi-fp50 in vivo

10 mice with subcutaneous Bxpc3 tumors were randomly divided into two groups (Bi-fp50 and scFv2). When the tumor size reached about 6 ~ 7 mm, Bi-fp50 (10 mg kg^{-1}) or scFv2 (10 mg kg^{-1}) was intravenously injected through the tail vein 2 times/week. And the mice's tumor size and body weight were recorded every 2 days after injection. The mice were sacrificed 21 days after treatment, and major organs were harvested, fixed in 4% neutral buffered formalin, embedded in paraffin, and sectioned for further histological analysis. To evaluate in-depth intra-tumoral treatment

effects, another 6 mice with Bxpc3 tumors were euthanized 3 days after different treatments (Bi-fp50 and scFv2, $n=3$). The whole tumors were collected and fixed in 4% PFA for 1 day. Then the Bxpc3 tumor tissues were transferred for TUNEL staining following the standard protocol.

Statistical analysis

All quantitative data were recorded as mean ± standard S.D. Means were compared using paired *t*-test and two-way analysis of variance (ANOVA). The Pearson test used linear and non-linear tests. $*p<0.05$ were considered as statistical significance; $**p<0.01$, remarkably; $***p<0.001$, very prominently.

Results

Synthesis and characteristics of Bi-fp50

The bispecific fusion protein Bi-fp50 was designed and synthesized by a typical synthetic biology strategy (Scheme 1 and Fig. S1). The molecule weight of purified Bi-fp50 and the corresponding scFvs were first evaluated by sodium dodecyl sulfate–polyacrylamide gel electrophoresis (SDS-PAGE) with 15% gel (Fig. 1A). The Bi-fp50 (purity of 92% by ultraviolet analysis) had an approximate molecular weight of 50 kDa. In contrast, the two corresponding scFv was about 30 kDa. The obtained Bi-fp50 also showed a typical 3D protein structure from the FTIR spectrum (Fig. 1B). It could be seen that 1334 cm^{-1} and 1750 cm^{-1} represented the β-sheet and β-turn structure of the 3D protein, respectively. Furthermore, from the enzyme-linked immunosorbent assay (ELISA) measurement, as shown in Fig. 1C and D, Bi-fp50 showed a high target binding capacity comparable to the anti-VEGF scFv or anti-EGFR scFv, respectively. It was also noted that Bi-fp50 could efficiently recognize both targets simultaneously in a dose-dependent manner (Fig. 1E).

In vitro *binding affinity of Bi-fp50*

To quantitatively evaluate the expression patterns in PDAC, six typical PDAC cell lines were first chosen for the western blotting assay (Fig. 2A). Anti-glyceraldehyde 3-phosphate dehydrogenase (GAPDH) antibodies were used as a loading control. All 6 cell lines showed relative solid abundance corresponding to moderate/high EGFR

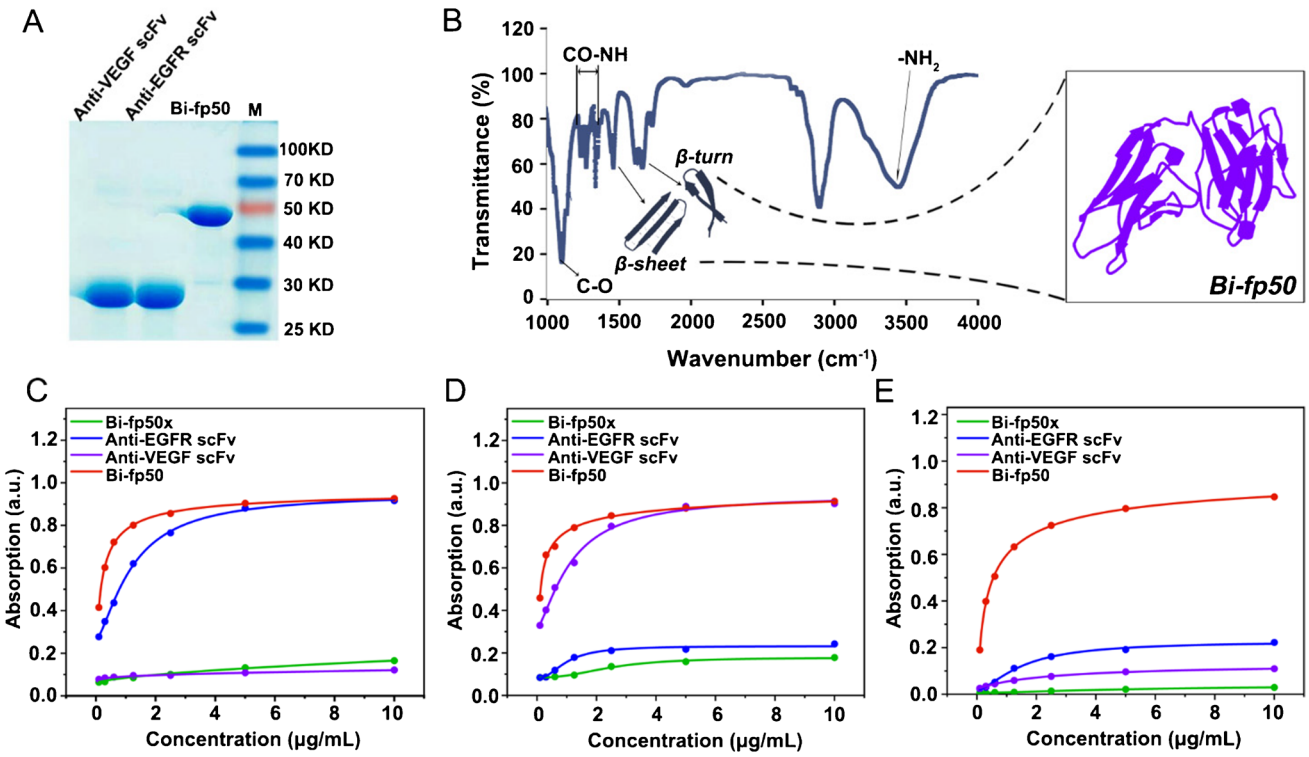

Fig. 1 Characterization and binding affinity assessment of the Bi-fp50. **A** SDS-PAGE analysis of the purified Bi-fp50 and two individual scFv. Bi-fp50 is about 50 kDa. B, Fourier-transform infrared spectroscopy (FTIR) spectrum of Bi-fp50 reflects some typical structures and groups of the protein. **C–E** The binding capacity of Bi-fp50 for EGFR (**C**), VEGF (**D**), EGFR, and VEGF simultaneously (**E**). Bi-fp50 shows a high affinity with human EGFR and VEGF

and VEGF overexpression. Further quantitative analysis showed that two cell lines with relatively higher EGFR and VEGF expression were Bxpc3 and Aspc1 (Fig. 2B and C). Therefore, we used these two cell lines in the subsequent investigation.

The in vitro binding affinity of Bi-fp50 in Bxpc3 cells was then evaluated after anti-EGFR scFv, anti-VEGF scFv, scFv2, Bi-fp50, and Bi-fp50x were labeled with AF488 (green fluorescence) dyes. As shown in Fig. 2D, two scFvs (anti-EGFR scFv, anti-VEGF scFv) had an apparent affinity for Bxpc3 cancer cells. ScFv2 group showed more intense fluorescence intensity with the Bxpc3 cells than each scFv, indicating an enhanced targeting effect. Similarly, the Bi-fp50 group had a significantly stronger green signal than single scFv groups, while the dual-blocking group had almost no fluorescence. Also, no green signal was observed in the Bi-fp50x and the corresponding dual-blocking group. Quantitative fluorescence analysis (Fig. 2E) showed that the scFv2 and Bi-fp50 groups had significantly stronger fluorescence than the separately anti-VEGF scFv and anti-EGFR scFv groups. The fluorescence intensity of scFv2 and Bi-fp50 was approximately equal to the sum of that of two individuals. These results proved the enhanced, accumulated binding capability of Bi-fp50 and scFv for PDAC cells in vitro. To further explore the location of two scFvs (or Bi-fp50) bind cells, anti-EGFR scFv-AF647 (red) and anti-VEGF scFv-AF488 (green) were incubated with Bxpc3 cells simultaneously; two different fluorescence were found matched (Fig. 2F), suggesting the colocalization of two targets on the Bxpc3 cell surface. Additionally, the same pathway of two fluorescence channels from the selected area (Fig. 2G) and high Pearson's r (PCC) of 0.97 (Fig. 2H) further demonstrated the excellent colocalization of VEGF and EGFR in Bxpc3 cancer cells.

In vitro *anticancer activity of Bi-fp50*

The anticancer activity of Bi-fp50 for PDAC cells was further investigated in vitro. The Live/Dead staining assay intuitively and qualitatively showed that more Bxpc3 cells were dead in Bi-fp50 and scFv2 groups than in anti-EGFR scFv, anti-VEGF scFv, scFv2, and Bi-fp50x groups under the same concentration and incubation time (Fig. 3A). Using untreated cells as a normalized control, anti-EGFR scFv, anti-VEGF scFv, and Bi-fp50 treated HPDE6-C7 cells which were human standard pancreatic duct epithelial cells with average level expression of EGFR, and VEGF (Fig. S2) showed only a slight effect on growth even at high concentrations (Fig. 3B). Therefore, Bi-fp50 is relatively safe for normal cells at a certain concentration. By contrast, Bi-fp50 significantly inhibited the proliferation and growth of Bxpc3 and Aspc1 PDAC cells even under a relatively low concentration of 0.3 μM (Fig. 3C and D), while anti-EGFR scFv and anti-VEGF scFv alone had only a relatively slight inhibitory effect at the same concentration. The half-maximal inhibitory concentration (IC_{50}) of Bi-fp50 to Bxpc3 and Aspc1 cells were about 0.32 μM and 0.38 μM, respectively, while the IC_{50} of the two individual scFv to PDAC cells was more than 1.0 μM (Fig. 3C and D). Flow cytometry assay of cell apoptosis (Fig. 3E) showed that Bi-fp50 treatment induced the early and late apoptosis of Bxpc3 cells (75.7%). The population of apoptotic cells was, 72.6% of scFv2, 67.7% of anti-EGFR scFv, and 55.7% of anti-VEGF scFv, respectively. Although enough anti-EGFR scFv and anti-VEGF scFv could inhibit Bxpc3 cells, owing to the overexpression of both EGFR and VEGF, they needed a longer time (48 h), reflecting the low therapeutic effect.

Blood clearance, biodistribution, and in vivo *tumor penetration of Bi-fp50*

Before being applied in vivo, the pharmacokinetics and biodistribution of Bi-fp50 protein were investigated. For visualization, the near-infrared fluorescent molecule IRDye 800CW (Dye800) was conjugated to Bi-fp50 and scFv2 (Fig. S3). The Bi-fp50-Dye800 or scFv2-Dye800 (control group) were intravenously injected into orthotopic Bxpc3 tumor-bearing mice. The half-life of blood clearance of Bi-fp50 was 4.33 ± 0.23 h. The area under the concentration–time curve (AUC) was 115 ID% h g^{-1} (Fig. 4A). This is like the pharmacokinetic profile of the small-sized protein molecules [30]. In vivo dynamic biodistribution of Bi-fp50-Dye800 in mice was directly observed by fluorescence imaging (Fig. 4B). Considerable fluorescence of Bi-fp50-Dye800 in PDAC tumors was observed from 2 h post-injection and gradually increased at tumor site from 4 to 12 h, indicating the continuous accumulation of Bi-fp50-Dye800. Ex vivo fluorescence images of 12 h post-injection further conformed to the significant enrichment of Bi-fp50-Dye800 in the tumor. A quantitative analysis of the fluorescence signal to background ratio (SBR) of the tumor showed that the SBR of Bi-fp50 reached 3.65 post-injection of 4 h (Fig. 4C) and continually increased to 3.73 in 8 h and maintained a higher value to 12 h, indicating the increased accumulation of probe in the tumor. In contrast, the enrichment of scFv2-Dye800 in the tumor was intuitively lower than that of Bi-fp50-Dye800 at different time points (Fig. 4B and C). The AUC (area under the curve) of SBR was 87.99 h for Bi-fp50-Dye800, nearly two times for scFv2-Dye800 (45.26 h). Furthermore, from the quantitative biodistribution analysis of the probe in tissues ($n=3$), Bi-fp50-Dye800 tended to be enriched in the kidney (4 h to 8 h). Then it was metabolized mainly from the kidney, while the scFv2-Dye800 showed higher accumulation in the liver (Fig. 4D and E), owing to the effect of protein size.

The photoacoustic imaging (PAI) was further carried out to evaluate the time-dependent penetration of Bi-fp50 into the tumor (Fig. S4). Bi-fp50-Dye800 gradually penetrated the

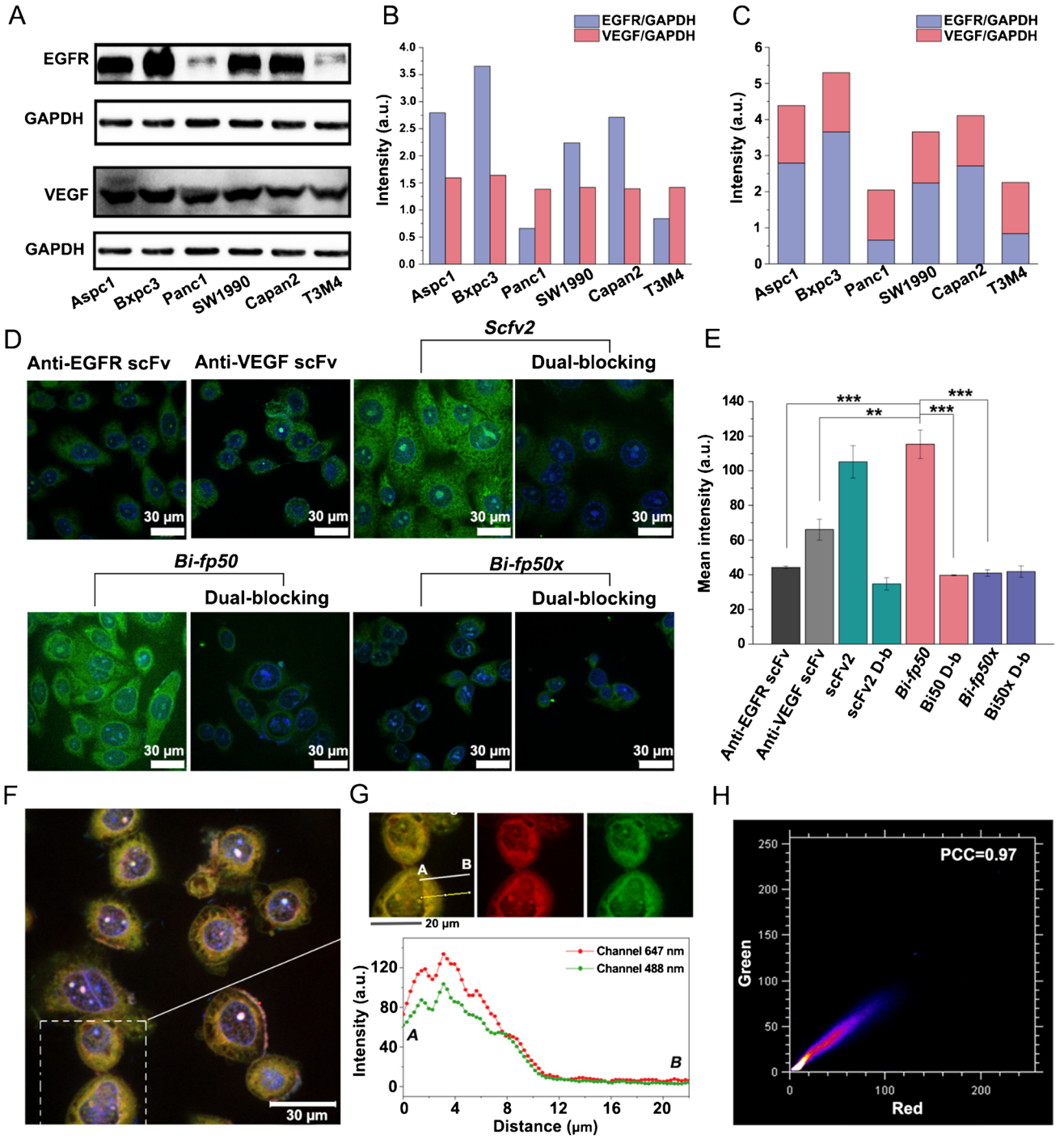

Fig. 2 In vitro targeting assessment of Bi-fp50. **A** Western blotting bands of EGFR and VEGF expression in different pancreatic cancer cell lines. GAPDH expression works as the standard inner line. **B**, **C** Quantitative analysis of EGFR and VEGF expression individually (**B**) or accumulated (**C**) in six cell lines. **D** Confocal images of Bxpc3 pancreatic cancer cells incubated with anti-EGFR scFv, anti-VEGF scFv, scFv2 (connected the two scFv), Bi-fp50, Bi-fp50x (negative control). The Alexa Fluor 488 dye (AF488) was conjugated to image the probes and corresponding dual-blocking as the control groups. **E** Quantitative analysis of the confocal images ($n = 3$). Data are presented as mean ± standard deviation (SD); ** $P < 0.01$, *** $P < 0.001$. **F** The confocal image of Bxpc3 cells was simultaneously incubated with anti-EGFR scFv-AF647 (red) and anti-VEGF scFv-AF488 (green). **G**, **H** Location analysis of simultaneous targeting of EGFR (red) and VEGF (green) in a single cell (**G**) and corresponding colocalization coefficient (**H**), indicating the colocalization of VEGF and EGFR on the Bxpc3 cell surfaces

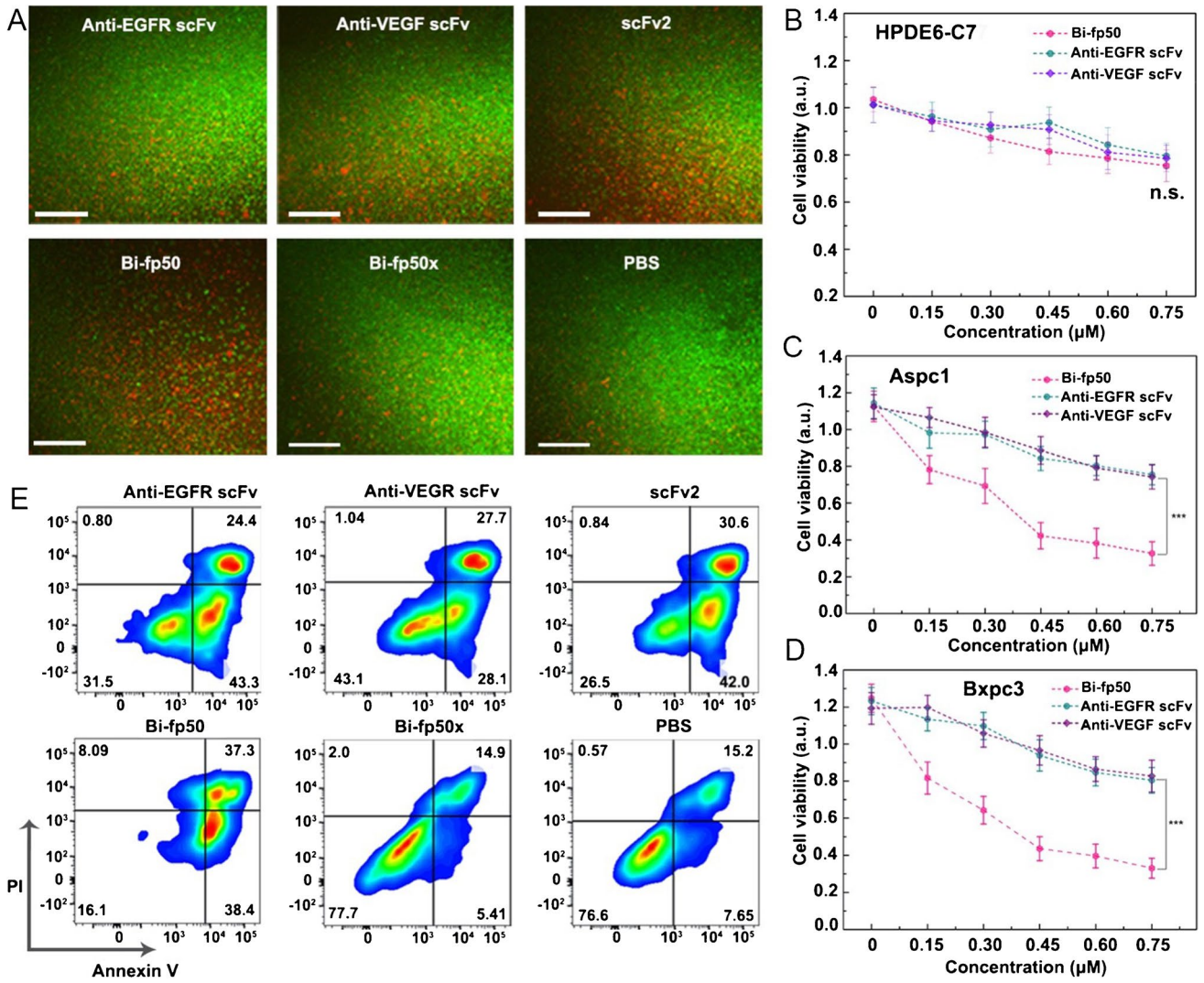

Fig. 3 In vitro anticancer activity of Bi-fp50. **A** Fluorescence images of Bxpc3 with different agents under the same concentration and time treatment (24 h) stained with Calcein AM (live cells, green) and BOBO-3 Iodide (dead cells, red). Scale bar, 200 μm. **B**–**D** Relative viability of Human Pancreatic Duct Epithelial Cell HPDE6-C7 (**B**), pancreatic cancer cell Aspc1 (**C**), and Bxpc3 cells (**D**) after co-incubated with anti-EGFR scFv, anti-VEGF scFc, and Bi-fp50 for 24 h. **E** Assessment of cellular death (apoptosis and necrosis) using Annexin V-FITC/PI staining after incubation with different probes of the same concentration for 48 h

surrounding tumor parenchyma from local tumor vasculature (Fig. 4F). In contrast, the PAI signal of scFv2-Dye800 protein was much weaker than that of Bi-fp50-Dye800 at all time points. The signals of Bi-fp50 reached their peak in 8 h (Fig. 4G), consistent with fluorescence intensities. Additionally, cross-sectional PAI images (Fig. S5) showed a clear tumor profile by the Bi-fp50 probe in the tumor section, while only blurred boundaries could be imaged under the scFv2-Dye800 probe.

In vivo *real-time tracking and locating Bi-fp50 in local pancreatic tumor*

We further evaluated the dynamic and precise biodistribution of systemically administered Bi-fp50 in tumor microenvironments by fiber-optic confocal fluorescence microscopy (CFL) [31, 32] in an orthotopic Bxpc3 pancreatic tumor model. Before injection of Bi-fp50 (labeled with AF647) or scFv2, FITC (fluorescein isothiocyanate, green) dyes were injected to visualize the normal pancreatic tissues, PDAC tumor. The junction of the peri-tumor and tumor tissues (Fig. 5A). Immediately after intravenous injection of Bi-fp50-AF647 or scFv2-AF647, more Bi-fp50 was enriched in tumor blood vessels than scFv2 (Fig. 5B). Furthermore, 8 h post-injection, Bi-fp50 was widely distributed throughout the deep tissue of the tumor (Fig. 5C and Fig. S6). At the same time, only a small fluorescence signal was observed in adjacent normal and junction tissue. In contrast, only a tiny part of scFv2 was

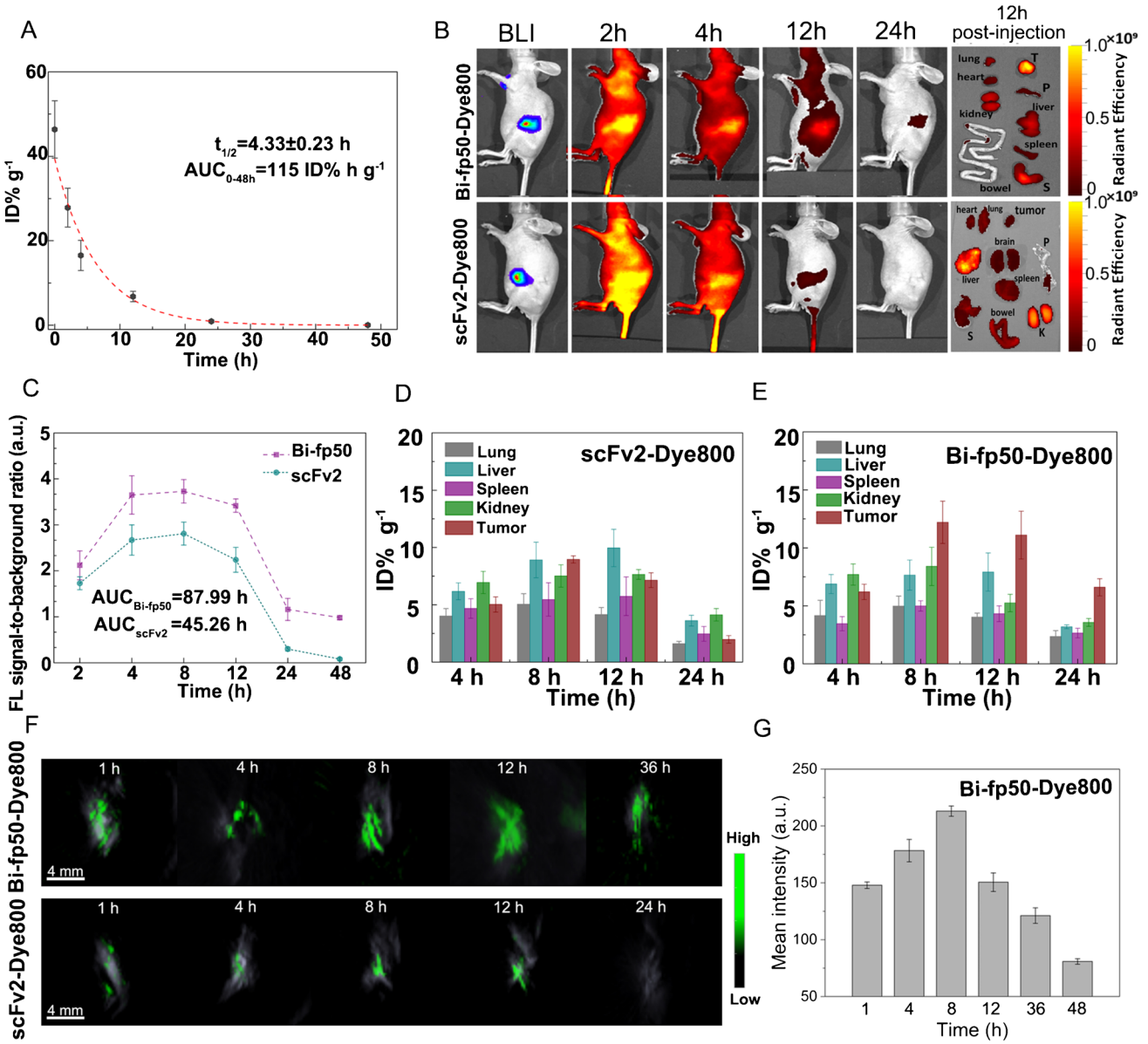

Fig. 4 Pharmacokinetic and biodistribution evaluation of Bi-fp50. **A** The blood circulation curve of the Bi-fp50-Dye800 was determined by measuring the dye800 fluorescence intensity in the blood of the orthotopic Bxpc3 tumor-bearing mice at different time points post intravenous injection ($n=3$). **B** In vivo fluorescence images of the Bi-fp50-Dye800 and scFv-Dye800-treated mice at different time points post intravenous injection. 12 h after injection, tumors and major organs were harvested for ex vivo imaging. S, stomach; P, pancreas; T, tumor. **C** Quantitative analysis of fluorescence intensity of Dye800 for Bi-fp50 and scFv2 in the tumor at different time points ($n=3$), the area of the small trapezoid under the curve is accumulated as AUC. **D**, **E** Quantitative biodistribution analysis of the scFv-Dye800 (**D**) and Bi-fp50-Dye800 (**E**) in mice (3 mice in each group) by measuring the Dye800 fluorescence intensity in the tumors and major organs at different times points post-injection. **F** 3D photoacoustic images of orthotopic Bxpc3 tumors were acquired at different time points after injection of Bi-fp50-Dye800 and scFv-Dye800 probes. The bright signals are from the blood vessels in the tumor owing to hemoglobin. The green signal corresponds to the distribution of probes. **G** Quantitative analysis of PAI intensity of tumor at different time points ($n=3$)

distributed in the deep tumor tissue, and a large proportion of scFv2 was concentrated in normal or junction areas (Fig. 5C and Fig. S6). The quantitative analysis of fluorescence intensity from CFL images confirmed such results and further revealed that the intensity of Bi-fp50 was about 2.5 times scFv2 in the deep tumor region and 1.7 times in the tumor of junction region (Fig. 5D). In addition, immunofluorescence (IF) images of the whole tumor section showed that the Bi-fp50 had penetrated the deep tumor tissue and distributed very uniformly across

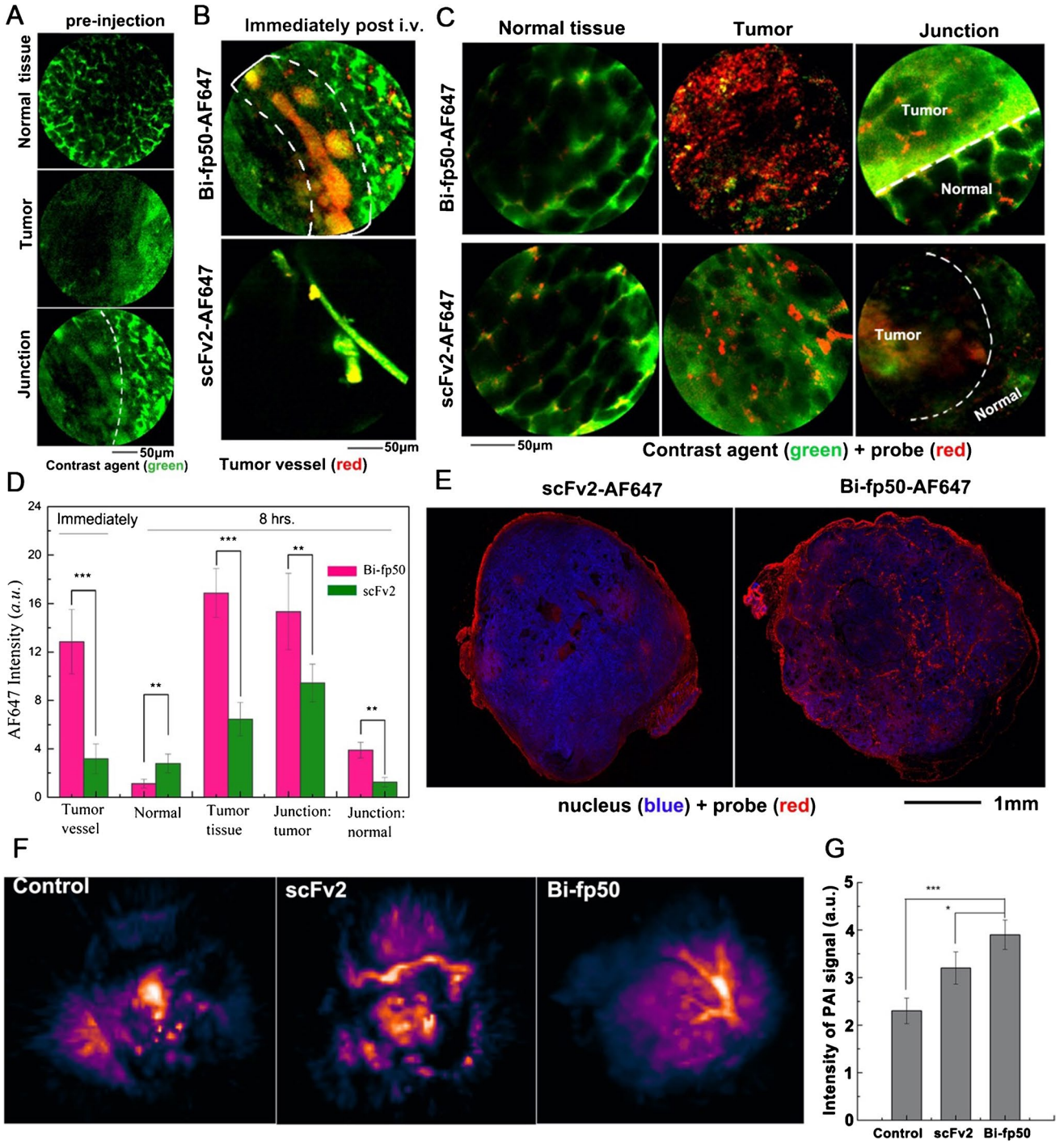

Fig. 5 In vivo real-time imaging of Bi-fp50 and scFv2 in tumor and vasculature of the orthotopic Bxpc3 tumor-bearing mice. **A** Confocal fluorescence laser-microscopy (CFL) images of tumor tissue, surrounding normal tissue, and the junction between them pre-injection of probes. Single FITC dyes (green) were injected for 30 min before imaging to visualize the outline of tissues. **B** CFL images of tumor tissue immediately post i.v. injection of probes (red). **C** CFL images of tumor, normal, and junction tissues 8 h post i.v. injection of probes (red). **D** Quantitative analysis of fluorescence intensity of Bi-fp50 or scFv2 in different positions of PDAC tumor at different time points ($n=3$). **E** Immunofluorescence (IF) images of the whole tumor tissues resected 8 h after intravenous injection of scFv2 or Bi-fp50. The probes were labeled with AF647 (red), and the nuclei were stained with 4′,6-diamidino-2-phenylindole (DAPI). **F** 3D photoacoustic images of orthotopic Bxpc3 tumors were acquired 12 h after different injections: PBS (control), scFv2, and Bi-fp50. The bright signals are from the blood vessels in the tumor owing to hemoglobin. Brightness is positively correlated with hemoglobin content and identifies the distribution of tumor micro-vessels. **G** Quantitative analysis of PAI signals ($n=3$). * $P<0.05$, ** $P<0.01$, *** $P<0.001$

the entire tumor, while scFv2 was mainly spread in the surface layer of the rich vasculature (Fig. 5E).

In addition to targeting PDAC cells, Bi-fp50 can also act on the tumor's vasculature by targeting the VEGF pathway to improve tumor vessel perfusion [23, 24]. The 3D PAI images of the orthotopic Bxpc3 pancreatic tumor showed that compared with the control group (non-treated) and the group injected with scFv2, the tumor vasculature of the Bi-fp50-treated group became significantly more abundant. In addition, the blood flow increased 12 h post-injection (Fig. 5F). The quantitative analysis of PAI signals further confirmed that the improvement of tumor perfusion of Bi-fp50 was more significant than the bispecific scFv2 (Fig. 5G).

In vivo *antitumor efficacy of Bi-fp50*

Encouraged by promising results of in vitro therapy and in vivo imaging, we further explored the antitumor efficacy of Bi-fp50 in vivo. 10 Balb/c nude mice with Bxpc3 xenograft pancreatic tumors were randomly divided into two groups ($n=5$). After intravenously injected with Bi-fp50 (10 mg kg^{-1}) or scFv2 (10 mg kg^{-1}), mice's tumor size and body weight were recorded every 2 days. The substrate to activate Luc-protein of Bxpc3 cells was administered through intraperitoneal injection to visualize the tumor size (Fig. 6A). After 3 weeks of treatment, the bioluminescence imaging (BLI) and the representative photographs of tumors showed that the tumor size in the Bi-fp50 group was smaller than that in the scFv2 group (Fig. 6A and C). Furthermore, the Bi-fp50 group showed a higher antitumor efficacy with a tumor inhibition ratio of 35.14% compared to the scFv2 group as a control (Fig. 6B), which indicated the therapeutic potential of Bi-fp50. The weight of the two groups of mice remained stable, and there was no significant difference (Fig. 6D). The antitumor efficiency was further evaluated by a terminal deoxynucleotidyl transferase-mediated deoxyuridine triphosphate nick end-labeling (TUNEL) assay. As shown in Fig. 6E, a few TUNEL-positive cells (green) were observed from the scFv2-treated tumor section. In contrast, many TUNEL-positive apoptotic cells (green) could be kept in the Bi-fp50-treated group and distributed throughout the entire tumor section. These results indicated that the Bi-fp50 could induce PDAC cell death by activating apoptosis in the tumor. After 3-week treatments, mice were sacrificed, and major organs (heart, liver, spleen, lung, kidney, and pancreas) were harvested for histological evaluation. The H&E staining showed no significant abnormalities and differences in major organs of Bi-fp50x (control) and Bi-fp50 groups (Fig. 6F).

After investigating the antitumor effect of Bi-fp50, the molecular mechanism underlying this effect was tentatively explored. We detected the activation of downstream molecules of EGFR and VEGF. In Bxpc3 cells, the constitutive phosphorylations of STAT3 and AKT signal pathways (P-STAT3, P-AKT) were more strongly inhibited by Bi-fp50 than other agents (scFv2, anti-EGFR scFv, anti-VEGF scFv, and Bi-fp50x) as shown in Fig. 6G and H. It has been reported that targeting EGFR and VEGF of PDAC cells will affect cell survival mainly through STAT3 and AKT pathways [13, 33]. Furthermore, inhibition of the expression of EGFR and downstream signaling pathways can induce apoptosis of pancreatic cancer cells, and downstream signaling pathways related to VEGF can affect cancer angiogenesis [34]. Therefore, the simultaneous binding of Bi-fp50 to EGFR and VEGF can crosstalk and regulate AKT and STAT3-related pathways together, thereby affecting the cell growth, survival, angiogenesis, and migration of PDAC cells (Fig. 6I).

Discussion

Pancreatic ductal adenocarcinoma (PDAC) is still one of the most lethal solid tumors and is predicted to be the second leading cause of cancer-related mortality in the next decade [12]. The overall 5-year survival for pancreatic cancer has changed little over the past few decades despite the improvements in palliative therapies and considerable progress in adjuvant and neoadjuvant treatment [35, 36]. These failures have been widely believed to relate to the high molecular heterogeneity and the surrounding nearly impenetrable desmoplastic stroma of PDAC [37]. Here, we developed an ultrasmall-sized, dual-targeted fusion protein Bi-fp50 probe that can efficiently penetrate and largely accumulate into dense orthotopic PDAC tumors and then targeted EGFR/VEGF simultaneously and induced noticeable therapeutic effects in vivo.

There had been much hope that specific pathway-targeted therapies, including antiangiogenic drugs bevacizumab or aflibercept [38, 39] and multikinase inhibitors sunitinib or sorafenib [40, 41], would yield improvements in outcomes, however, end with non-statistically significant effects in clinic. The high molecular heterogeneity of PDAC tumors is believed to be one of the main reasons. Multispecific targeting agents have been found to effectively reduce the impact of cancer cell heterogeneity and improve drug efficacy in various cancer [12]. For PDAC cells, EGFR and VEGF are not only overexpressed in more than 90% and 64% of patients' PDAC separately, but also, they are interrelated, and dual EGFR-VEGF pathway inhibition could delay acquired resistance of anti-EGFR or anti-VEGF used alone [20–22]. Therefore, we hope to construct bispecific probes that can simultaneously target EGFR and VEGF to achieve better therapeutic effects in vivo, which has not been reported on PDAC. The obtained Bi-fp50 showed an excellent simultaneous binding affinity for EGFR and VEGF with good colocalization performance in Bxpc3 PDAC cells. The half-maximal inhibitory concentration (IC_{50}) of Bi-fp50 to Bxpc3 and Aspc1 PDAC cells was about 0.32 μM, just one-third of the two individual scFv. The fusion bispecific Bi-fp50

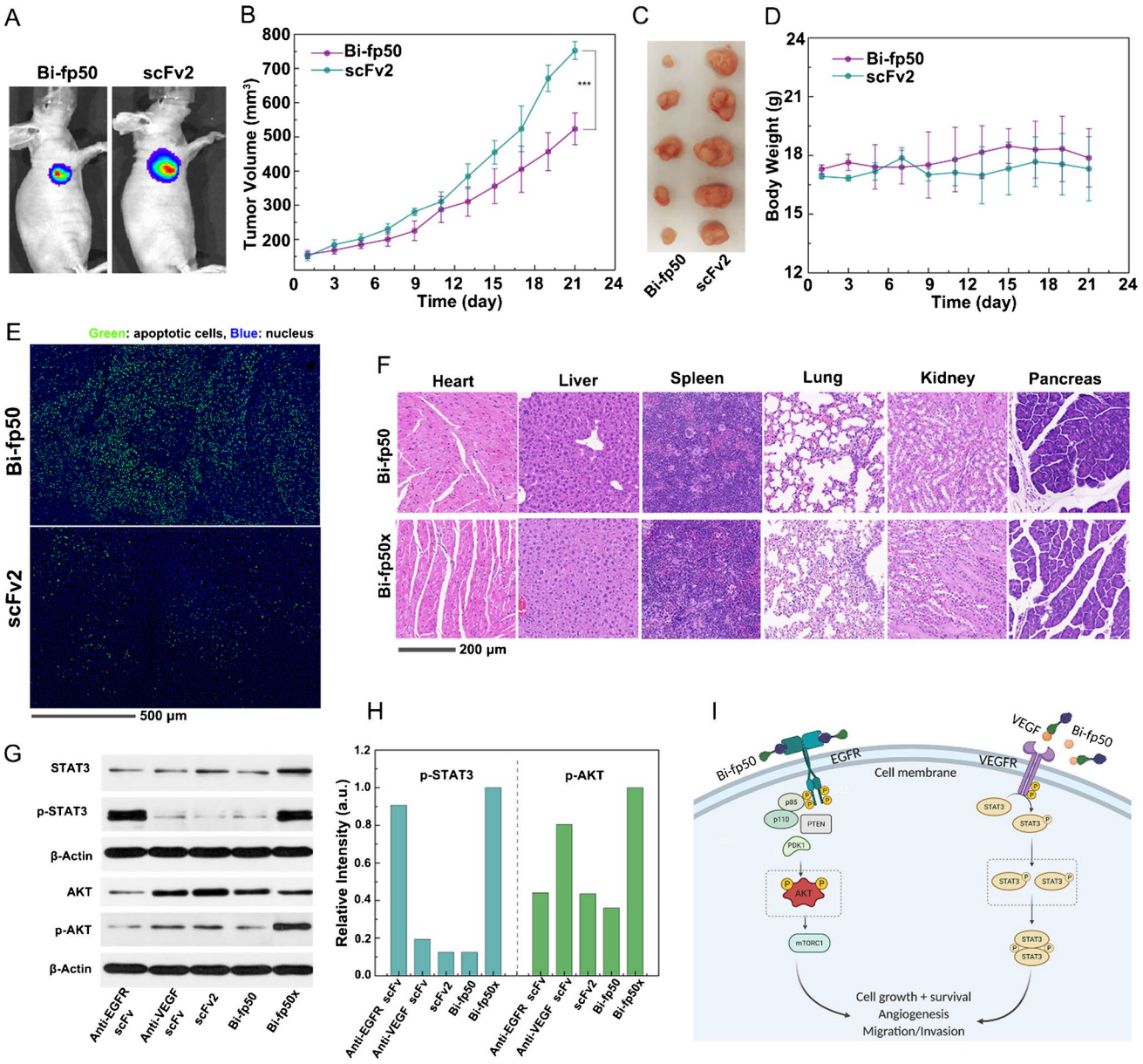

Fig. 6 In vivo evaluation of antitumor efficacy of Bi-fp50. **A** Bioluminescence imaging (BLI) of xenograft Bxpc3 tumor-bearing mice 3 weeks after different treatments. **B** Growth curves of Bxpc3 tumors in different groups of nude mice treated with Bi-fp50 or scFv2 with a dose of 10 mg kg^{-1}. Data are mean ± s.d. of biological replicates ($n = 5$). *** $p < 0.001$. **C** Tumors were dissected on day 22 for the Bi-fp50 and scFv2 groups. **D** Body weights of mice in different groups 3 weeks after treatments. Data are mean ± s.d. of biological replicates ($n = 5$). **E** TUNEL (terminal deoxynucleotidyl transferase-mediated deoxyuridine triphosphate nick-end labeling)-stained tumor Sects. 5 days after different treatments ($n = 3$). Apoptotic cells are shown in green. **F** H&E staining of major organs 3 weeks after Bi-fp50 and Bi-fp50x (negative control) treatment. **G** Western blotting bands of STAT3 and AKT signal pathway. β-Actin was the standard inner line. **H** The relative intensity of p-STAT3 and p-AKT proteins. **I** Schematic illustration of the main inhibition mechanism of Bi-fp50 in EGFR and VEGF signal for PDAC

showed an excellent or synergistically enhanced therapeutic effect relative to two individual scFv in vitro.

Moreover, PDAC is characterized by nearly impenetrable desmoplastic stroma barriers, hypoperfused and hypovascular tumor vessels, and high intra-tumoral fluid pressure that enriches and infiltrates large-sized probes very difficult [12, 42]. Therefore, the size of the therapeutic agent is one of the keys to restricting the drug's action. According to a previous analysis of protein diameter [29, 30], the hydrodynamic diameter of the Bi-fp50 is estimated about 5 ~ 6 nm, which is very conducive to the penetration of the probe in the high-density PDAC tumors and timely renal clearing from the

body [13]. The ultra-small size allows Bi-fp50 to penetrate deeper tissues, thereby altering the broader vascular system. The increase of vascular permeability can, in turn, promote the penetration of Bi-fp50. Thus, the interaction of ultra-small size and anti-VEGF capability allows for better penetration and distribution of Bi-fp50. The significant penetration and uniform distribution of Bi-fp50 in tumor tissues lay the foundation for the exertion of bispecific therapeutic effects. Additionally, the ultrasmall size allowed the Bi-fp50 to be quickly cleared from the body through the kidneys, making it more suitable for in vivo imaging and therapy, especially given the long-term safety profile [13, 30].

After intravenous injection, the Bi-fp50 protein significantly inhibited PDAC tumor growth in vivo without other noticeable side effects. It should be noted that in the xenograft PDAC tumor model, Bi-fp50 did not have a complete inhibition effect, partially owing to just conducting a twice injection/treatment per week. Actually, it is almost impossible for this extremely stubborn PDAC tumor to achieve a full therapeutic effect with a single treatment method. In addition to the terminal groups targeting EGFR and VEGF, there are still accessible positions of Bi-fp50 where more molecular-scale therapeutic factors can be connected, such as radiotherapy and chemotherapy molecules [43, 44], to obtain a synergistic therapeutic effect.

Moreover, multispecific biological molecules, especially bispecific antibodies and their derivatives scFvs, can provide off-the-shelf immune therapeutics for treating cancer, which may solve the long-standing problems in this field [45–47]. As with any immunotherapy, safety and off-target toxicity issues are potential concerns. It has been proved that bispecific antibodies or derivatives that bridge T cell-cancer cells with two terminals of high-specific selectivity simultaneously can significantly decrease the risk of off-target side effects [16]. In addition, the intratumoral enrichment, penetration, and timely clearance from the body are critical for multispecific biological molecules when this strategy is applied to solid tumors and incredibly dense PDACs. Therefore, we believe that the Bi-fp50, with its ultra-small size and multi-specificity, will give massive potential in PDAC dual-targeted immunotherapy.

Conclusion

We constructed the bispecific fusion protein Bi-fp50 that could simultaneously target both EGFR and VEGF of PDAC cells. Due to the crosstalk and inter-regulation of the EGFR-VEGF pathway, the Bi-fp50 achieved an enhanced, synergistic therapeutic effect in Bxpc3 and Aspc1 PDAC cells. Furthermore, the Bi-fp50 largely penetrated dense barriers and enriched the whole Bxpc3 pancreatic tumor to achieve a significant tumor inhabitation effect in vivo. The synthesized Bi-fp50 showed excellent potential as an efficient pathway-targeted specific therapy for PDAC used alone or in combination with other therapeutic modalities.

Supplementary Information The online version contains supplementary material available at https://doi.org/10.1007/s00259-023-06115-5.

Acknowledgements We thank the technical support from the Multimodal Biomedical Imaging lab, the Institute of Automation, the Chinese Academy of Sciences, and the Cold Spring Biotech Co., Ltd. In addition, we thank Beijing Gegen Biotechnology Co., Ltd. for helping prepare and purify the scFv fragments and fusion protein. This work was supported by the National Key Research and Development Program of China (No. 2017YFA0205200), the National Natural Science Foundation of Youth Program of China (No. 81901813), and the CAMS Innovation Fund for Medical Sciences (No.2021-I2M-C&T-B-067). We also thank "BioRender" for the scheme organizing. Finally, H.Y. and S.H.Y. acknowledge support from the National Institutes of Health in the U.S. (R01-CA192878).

Author contribution Q.W., H.Y., J.T., and X.M.Z. discusses and convinced this project. H.Y. and Q.W. designed the experiments. Q.W. and Z.L. fabricated the Bi-fp50 protein. Q.W. and J.Y.W. performed the characterization, in vitro imaging, and therapy assessment. Q.W. developed the PDAC animal model. Q.W. and K.W. performed in vivo imaging experiments. Q.W. and J.Y.W. performed in vivo therapy experiments. F.Y.K. assisted in data analysis. Q. W., J.Y.W., and H.Y. prepared figures and wrote the manuscript with inputs from all co-authors.

Data Availability The data that support the figures within this paper is available upon reasonable request.

Declarations

Ethics approval The current study does not include any studies associated with human participants. All animal studies were performed according to the guidelines of the Animal Care Committee of the Chinese Academy of Medical Sciences Tumor Hospital.

Conflict of interest The authors declare no conflict of interest.

References

1. Siegel RL, Miller KD, Fuchs HE, Jemal A. Cancer Statistics, 2021. CA Cancer J Clin. 2021;71:7–33.
2. Mizrahi JD, Surana R, Valle JW, Shroff RT. Pancreatic cancer. Lancet. 2020;395:2008–20.
3. Christenson ES, Jaffee E, Azad NS. Current and emerging therapies for patients with advanced pancreatic ductal adenocarcinoma: a bright future. Lancet Oncol. 2020;21:e135–45.
4. Neoptolemos JP, Kleeff J, Michl P, Costello E, Greenhalf W, Palmer DH. Therapeutic developments in pancreatic cancer: current and future perspectives. Nat Rev Gastroenterol Hepatol. 2018;15:333–48.
5. Tempero MA. NCCN Guidelines Updates: Pancreatic Cancer. J Natl Compr Canc Netw. 2019;17:603–5.
6. Rashid NU, Peng XL, Jin C, Moffitt RA, Volmar KE, et al. Purity Independent Subtyping of Tumors (PurIST), A Clinically Robust, Single-sample Classifier for Tumor Subtyping in Pancreatic Cancer. Clin Cancer Res. 2020;26:82–92.

7. Collisson EA, Bailey P, Chang DK, Biankin AV. Molecular subtypes of pancreatic cancer. Nat Rev Gastroenterol Hepatol. 2019;16:207–20.
8. Shi Y, Gao W, Lytle NK, Huang P, Yuan X, Dann AM, et al. Targeting LIF-mediated paracrine interaction for pancreatic cancer therapy and monitoring. Nature. 2019;569:131–5.
9. Li YJ, Wu JY, Wang JM, Hu XB, Cai JX, Xiang DX. Gemcitabine loaded autologous exosomes for effective and safe chemotherapy of pancreatic cancer. Acta Biomater. 2020;101:519–30.
10. Deplanque G, Demarchi M, Hebbar M, Flynn P, Melichar B, et al. A randomized, placebo-controlled phase III trial of masitinib plus gemcitabine in the treatment of advanced pancreatic cancer. Ann Oncol. 2015;26:1194–200.
11. O'Neil BH, Scott AJ, Ma WW, Cohen SJ, Aisner DL, et al. A phase II/III randomized study to compare the efficacy and safety of rigosertib plus gemcitabine versus gemcitabine alone in patients with previously untreated metastatic pancreatic cancer. Ann Oncol. 2016;27:1180.
12. Ho WJ, Jaffee EM, Zheng L. The tumour microenvironment in pancreatic cancer — clinical challenges and opportunities. Nat Rev Clin Oncol. 2020;17:527–40.
13. Adiseshaiah PP, Crist RM, Hook SS, McNeil SE. Nanomedicine strategies to overcome the pathophysiological barriers of pancreatic cancer. Nat Rev Clin Oncol. 2016;13:750–65.
14. Deshaies RJ. Multispecific drugs herald a new era of biopharmaceutical innovation. Nature. 2020;580:329–38.
15. Weidanz J. Targeting cancer with bispecific antibodies. Science. 2021;371:996–7.
16. D. Slaga, D. Ellerman, T.N. Lombana, R. Vij, J. Li, et al. Avidity-based binding to HER2 results in selective killing of HER2-overexpressing cells by anti-HER2/CD3. Sci Transl Med. 2018; 10: eaat5775.
17. Yin W, Zhu J, Gonzalez-Rivas D, Okumura M, Rocco G, et al. Construction of a Novel Bispecific Antibody to Enhance Antitumor Activity against Lung Cancer. Adv Mater. 2018;30:1805437.
18. Cox AD, Fesik SW, Kimmelman AC, Luo J, Der CJ. Drugging the undruggable RAS: Mission Possible? Nat Rev Drug Discov. 2014;13:828–51.
19. Goel HL, Mercurio AM. VEGF targets the tumour cell. Nat Rev Cancer. 2013;13:871–82.
20. Tortora G, Ciardiello F, Gasparini G. Combined targeting of EGFR-dependent and VEGF-dependent pathways: rationale, preclinical studies and clinical applications. Nat Clin Pract Oncol. 2008;5:521–30.
21. Hung MS, Chen IC, Lin PY, Lung JH, Li YC, Lin YC, et al. Epidermal growth factor receptor mutation enhances expression of vascular endothelial growth factor in lung cancer. Oncol Lett. 2016;12:4598–604.
22. Saito H, Fukuhara T, Furuya N, Watanabe K, Sugawara S, et al. Erlotinib plus bevacizumab versus erlotinib alone in patients with EGFR-positive advanced non-squamous non-small-cell lung cancer (NEJ026): interim analysis of an open-label, randomised, multicentre, phase 3 trial. Lancet Oncol. 2019;20:625–35.
23. Jain RK. Normalization of Tumor Vasculature: An Emerging Concept in Antiangiogenic Therapy. Science. 2005;307:58–62.
24. Tong RT, Boucher Y, Kozin SV, Winkler F, Hicklin DJ, Jain RK. Vascular Normalization by Vascular Endothelial Growth Factor Receptor 2 Blockade Induces a Pressure Gradient Across the Vasculature and Improves Drug Penetration in Tumors. Cancer Res. 2004;64:3731–6.
25. Erkan M, Hausmann S, Michalski CW, Fingerle AA, Dobritz M, Kleeff J, Friess H. The role of stroma in pancreatic cancer: diagnostic and therapeutic implications. Nat Rev Gastroenterol Hepatol. 2012;9:454–67.
26. Cabral H, Matsumoto Y, Mizuno K, Chen Q, Murakami M, et al. Accumulation of sub-100 nm polymeric micelles in poorly permeable tumours depends on size. Nat Nanotechnol. 2011;6(12):815–23.
27. Wang Q, Yan H, Jin Y, Wang Z, Huang W, et al. A novel plectin/integrin-targeted bispecific molecular probe for magnetic resonance/near-infrared imaging of pancreatic cancer. Biomaterials. 2018;183:173–84.
28. Wang Q, Yan H, Wang Z, Li Z, et al. Construction of a novel bispecific fusion protein to enhance targeting for pancreatic cancer imaging. Biomaterials. 2020;255: 120161.
29. Tang L, Yang X, Yin Q, Cai K, Wang H, Chaudhury I, et al. Investigating the optimal size of anticancer nanomedicine. Proc Natl Acad Sci. 2014;111:15344–9.
30. H. Soo Choi, W. Liu, P. Misra, E. Tanaka, J.P. Zimmer, B. Itty Ipe, M.G. Bawendi, J.V. Frangioni. Renal clearance of quantum dots. Nat Biotechnol. 2007; 25: 1165–1170.
31. Ogata G, Ishii Y, Asai K, Sano Y, Nin F, Yoshida T, et al. A microsensing system for the in vivo real-time detection of local drug kinetics. Nat Biomed Eng. 2017;1:654–66.
32. Fan Z, Sun L, Huang Y, Wang Y, Zhang M. Bioinspired fluorescent dipeptide nanoparticles for targeted cancer cell imaging and real-time monitoring of drug release. Nat Nanotechnol. 2016;11:388–94.
33. Le X, Nilsson M, Goldman J, Reck M, Nakagawa K, et al. Dual EGFR-VEGF Pathway Inhibition: A Promising Strategy for Patients With EGFR-Mutant NSCLC. J Thorac Oncol. 2021;16:205–15.
34. Lu Z, Weniger M, Jiang K, Boeck S, Zhang K, Bazhin A, Miao Y, Werner J, D'Haese JG. Therapies Targeting the Tumor Stroma and the VEGF/VEGFR Axis in Pancreatic Ductal Adenocarcinoma: a Systematic Review and Meta-Analysis. Target Oncol. 2018;13:447–59.
35. Von Hoff DD, Ervin T, Arena FP, Chiorean EG, et al. Increased Survival in Pancreatic Cancer with nab-Paclitaxel plus Gemcitabine. N Engl J Med. 2013;369:1691–703.
36. Gunturu KS, Yao X, Cong X, Thumar JR, Hochster HS, Stein SM, Lacy J. FOLFIRINOX for locally advanced and metastatic pancreatic cancer: single institution retrospective review of efficacy and toxicity. Med Oncol. 2012;30:361.
37. Grünwald BT, Devisme A, Andrieux G, Vyas F, et al. Spatially confined sub-tumor microenvironments in pancreatic cancer. Cell. 2021;184:5577-5592.e18.
38. Kindler HL, Niedzwiecki D, Hollis D, Sutherland S, et al. Gemcitabine Plus Bevacizumab Compared With Gemcitabine Plus Placebo in Patients With Advanced Pancreatic Cancer: Phase III Trial of the Cancer and Leukemia Group B (CALGB 80303). J Clin Oncol. 2010;28:3617–22.
39. Rougier P, Riess H, Manges R, Karasek P, Humblet Y, et al. Randomised, placebo-controlled, double-blind, parallel-group phase III study evaluating aflibercept in patients receiving first-line treatment with gemcitabine for metastatic pancreatic cancer. Eur J Cancer. 2013;49:2633–42.
40. Kindler HL, Ioka T, Richel DJ, Bennouna J, et al. Axitinib plus gemcitabine versus placebo plus gemcitabine in patients with advanced pancreatic adenocarcinoma: a double-blind randomised phase 3 study. Lancet Oncol. 2011;12:256–62.
41. Kindler HL, Wroblewski K, Wallace JA, et al. Gemcitabine plus sorafenib in patients with advanced pancreatic cancer: a phase II trial of the University of Chicago Phase II Consortium. Invest New Drugs. 2012;30:382–6.
42. Chen X, Zeh HJ, Kang R, Kroemer G, Tang D. Cell death in pancreatic cancer: from pathogenesis to therapy. Nat Rev Gastroenterol Hepatol. 2021;18:804–23.
43. Fang J, Feng L, Meng L, Wang X, Liu H, et al. A novel ^{18}F-labeled agonist for PET imaging of stimulator of interferon gene expression in tumor-bearing mice. Eur J Nucl Med Mol Imaging. 2022;50:27–37.
44. Li C, Liu J, Yang X, Yang Q, Huang W, et al. Theranostic application of ^{64}Cu/^{177}Lu-labeled anti-Trop2 monoclonal antibody in pancreatic cancer tumor models. Nucl Med Mol Imaging. 2022;50:168–83.
45. S.C. Lee, J.S.Y. Ma, M.S. Kim, et al. A PSMA-targeted bispecific antibody for prostate cancer driven by a small-molecule targeting ligand. Sci Adv. 2021; 7: eabi8193.
46. Seung E, Xing Z, Wu L, Rao E, et al. A trispecific antibody targeting HER2 and T cells inhibits breast cancer growth via CD4 cells. Nature. 2022;603:328–34.
47. Brinkmann U, Kontermann RE. Bispecific antibodies. Science. 2021;372:916–7.

Authors and Affiliations

Qian Wang[1] · Jingyun Wang[2] · Hao Yan[3,6] · Zheng Li[4] · Kun Wang[5] · Feiyu Kang[6] · Jie Tian[5] · Xinming Zhao[1] · Seok-Hyun Yun[3]

1 Department of Diagnostic Imaging, National Cancer Center/National Clinical Research Center for Cancer/ Cancer Hospital, Chinese Acadamy of Medical Sciences and Peking Union Medical College, Beijing 100021, People's Republic of China

2 School of Pharmaceutical Sciences, Tsinghua University, Beijing 100084, People's Republic of China

3 Harvard Medical School and Wellman Center for Photomedicine, Massachusetts General Hospital, Cambridge, MA 02139, USA

4 Yi-Chuang Institute of Biotechnology Industry, Beijing 101111, People's Republic of China

5 CAS Key Laboratory of Molecular Imaging, Institute of Automation and Chinese Academy of Sciences, Beijing 100190, People's Republic of China

6 Tsinghua Shenzhen International Graduate School, Tsinghua University, Shenzhen 518055, People's Republic of China